Magnetic Resonance in Medicine 66:192–198 (2011)

Temporal Filtering Effects in Dynamic Parallel MRI

Martin Blaimer,[1]* Irene P. Ponce,[2] Felix A. Breuer,[1] Peter M. Jakob,[1,2] Mark A. Griswold,[3] and Peter Kellman[4]

Autocalibrated parallel MRI methods such as TSENSE or *k-t* SENSE have been presented for dynamic imaging studies as they are able to provide images with high temporal resolution. One key element of these techniques is the temporal averaging of the undersampled raw data to obtain an unaliased image. This image represents the temporal average (also known as direct current, DC) and is used to derive the reconstruction parameters. In this work, we show that aliasing artifacts can be introduced in the DC signal obtained from the undersampled raw data. These artifacts lead to undesired temporal filtering effects when the DC signal is used for coil sensitivity calibration or when the DC signal is subtracted from the raw data. It is demonstrated that the temporal filtering effects can be reduced significantly by filtering the DC signal. Magn Reson Med 66:192–198, 2011. © 2011 Wiley-Liss, Inc.

Key words: dynamic MRI; parallel MRI; GRAPPA; TSENSE; *k-t* SENSE; temporal filtering

A significant scan time reduction and thus higher frame rates in dynamic imaging can be achieved by parallel MRI (pMRI) methods. Dedicated reconstruction algorithms [e.g., sensitivity encoding (SENSE) (1), generalized autocalibrating partially parallel acquisitions (GRAPPA) (2)] use spatial coil sensitivity variations in an array of multiple receiver coils to obtain artifact-free images from undersampled raw data.

Autocalibrated dynamic pMRI techniques such as TSENSE (3), TGRAPPA (4), *k-t* SENSE (5), or *k-t* GRAPPA (6) use time interleaved acquisition schemes (also known as *k-t* sampling). For example, in TSENSE an unaliased image with full resolution is derived by temporal averaging of the aliased images. This image represents the temporal average (also referred to as direct current, DC) and is used to calculate the spatial coil sensitivity maps that are required for image reconstruction. However, in TSENSE undesired temporal filtering effects in the form of signal nulls in the temporal frequency spectra of the reconstructed dynamic images have been observed (7).

[1]Department of Diagnostic Imaging, Research Center Magnetic Resonance Bavaria (MRB), Würzburg, Germany.

[2]Department of Experimental Physics 5, University of Würzburg, Würzburg, Germany.

[3]Department of Radiology, University Hospitals of Cleveland and Case Western Reserve University, Cleveland, Ohio, USA.

[4]Laboratory of Cardiac Energetics, National Institutes of Health, National Heart, Lung and Blood Institute, Bethesda, Maryland, USA.

*Correspondence to: Martin Blaimer, Ph.D., Research Center Magnetic Resonance Bavaria (MRB), Am Hubland, 97074 Würzburg, Germany.
E-mail: blaimer@mr-bavaria.de

Received 21 April 2010; revised 29 November 2010; accepted 6 December 2010.

DOI 10.1002/mrm.22795
Published online 17 February 2011 in Wiley Online Library (wileyonlinelibrary.com).

The TGRAPPA (4) method works analogous to TSENSE except for its use of a relatively low order *k* space fitting for data reconstruction. In contrast to TSENSE, TGRAPPA does not exhibit temporal filtering of the dynamic images series but the signal-to-noise ratio (SNR) of the reconstructed images may be reduced.

Additionally, *k-t* SENSE (5) has been presented for dynamic imaging. In addition to pure coil sensitivity encoding, a priori information about spatio-temporal correlations is included in the reconstruction. The a priori information is typically obtained from fully encoded training data that is acquired by extra prescans or by using a variable density (VD) acquisition scheme (i.e., the central *k* space lines are fully encoded, whereas the peripheral *k* space is undersampled). In the original *k-t* SENSE approach, the DC is subtracted from the raw data so that only the dynamics of the object are reconstructed. In that way, the number of overlapping signal containing pixels is reduced by removing static pixels (8). However, undesired temporal filtering effects have also been observed in *k-t* SENSE reconstructions (8,9). In particular, signal nulls have been observed in the temporal frequency spectra of *k-t* SENSE images (10,11) analogous to TSENSE.

In this work, we describe the origin of the signal nulls and demonstrate that the temporal filtering effects in TSENSE and *k-t* SENSE can be reduced significantly when the DC is filtered by an additional GRAPPA reconstruction.

THEORY

Relationship between Data Sampling and the DC Signal

For a two-dimensional dynamic imaging experiment with phase encoding along the k_y direction and readout along the k_x direction, the sampling function $E(k_x,k_y,t)$ describes how *k* space is sampled over time *t*. It is a discrete delta function with unity values at sample locations and zero elsewhere (see Fig. 1a). In the following, we assume that the temporal signal is band-limited and is sampled adequately (i.e., has high enough image frame rate) to represent the maximum temporal frequency content. To investigate temporal filtering effects, it is useful to represent the dynamics of the object in $\boldsymbol{r}$-f space. Here, the vector $\boldsymbol{r} = (x,y)$ describes the spatial coordinates within the field-of-view (FOV) in the image and f represents a temporal frequency. For a time-interleaved sampling scheme with acceleration factor R, the measured object $\rho_{sub}(x,y,f)$ in $\boldsymbol{r}$-f space is given by the convolution of the fully sampled object $\rho_{full}(x,y,f)$ and the point-spread function, PSF = FT($E(k_x,k_y,t)$), where FT represents a Fourier transform (see Fig. 1a,b):

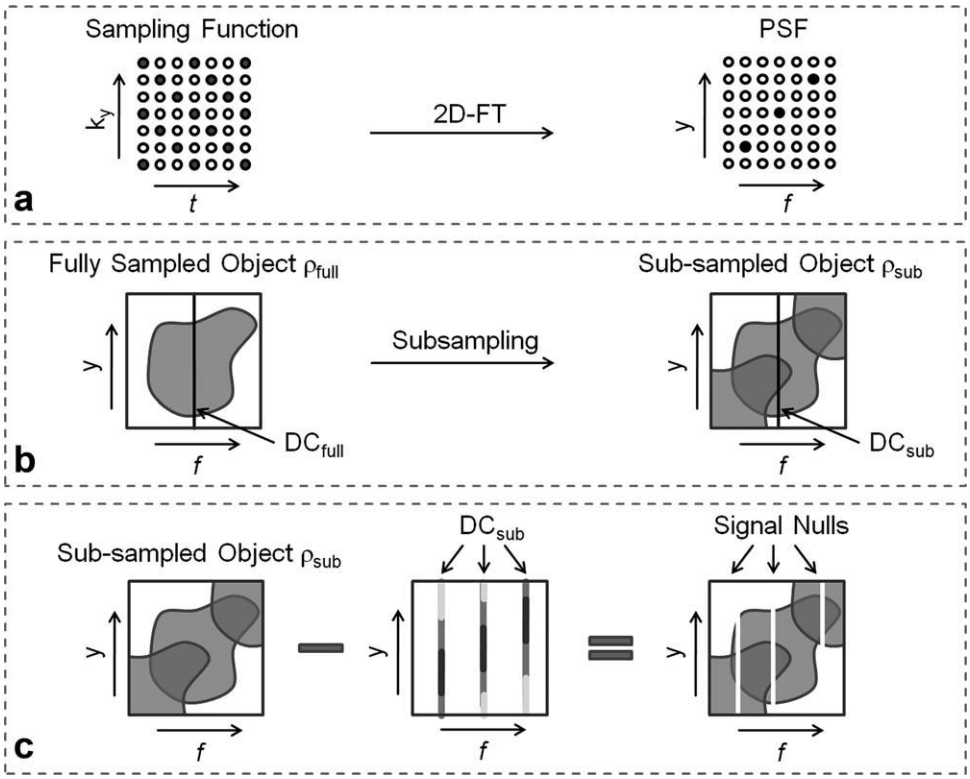

FIG. 1. Schematic illustrating the relationship between data sampling and errors in the temporal average (also referred to as DC). **a**: The sampling function describes those k_y-t positions where data is sampled. In this example, the data set is subsampled by a factor of $R = 3$. Filled circles represent sampled data and unfilled circles represent not sampled data. The 2D Fourier transform (FT) of the sampling function yields the PSF. According to the PSF, a signal in y-f space will be the superposition of $R = 3$ signals in this example. **b**: For a fully sampled data set, the unaliased object can be represented in the y-f space and the unaliased DC_{full} signal can be obtained at temporal frequency $f = 0$. However, when subsampling is performed, aliasing occurs in y-f space. The aliasing pattern is thereby determined by the PSF. As one can see, for the subsampled data the DC_{sub} signal at $f = 0$ is the superposition of DC_{full} and $R - 1$ additional signal components. **c**: According to the PSF multiple shifted replica of DC_{sub} exist in y-f space. Therefore, when DC_{sub} is subtracted from the subsampled raw data, signal nulls at R temporal frequency positions are generated in y-f space.

$$\rho_{\text{sub}}(x,y,f) = \text{PSF}(x,y,f) * \rho_{\text{full}}(x,y,f) = \sum_{n=0}^{R-1} \rho_{\text{full}}\left(x, y - n \cdot \tfrac{\text{FOV}}{R}, f - n \cdot \tfrac{f_{\max}}{R}\right) \quad [1]$$

The maximum sampled temporal frequency is given by $f_{\max}$. The symbol * represents a convolution.

In dynamic pMRI, the DC is typically obtained by temporal averaging of the subsampled raw data. In ***r***-f space, the DC corresponds to the signal at temporal frequency $f = 0$ and according to Eq. 1 it can be written as:

$$DC_{\text{sub}}(x,y) = \rho_{\text{sub}}(x,y,f=0) = \sum_{n=0}^{R-1} \rho_{\text{full}}\left(x, y - n \cdot \tfrac{\text{FOV}}{R}, -n \cdot \tfrac{f_{\max}}{R}\right) \quad [2]$$

Thus, $DC_{sub}(x,y)$ is the superposition of the DC signal from the fully sampled acquisition $DC_{full}(x, y) = \rho_{full}(x, y, f = 0)$ and signals from different locations within the FOV as well as from different temporal frequencies:

$$DC_{\text{sub}}(x,y) = DC_{\text{full}}(x,y) + \sum_{n=1}^{R-1} \rho_{\text{full}}(x, y - n \cdot \tfrac{\text{FOV}}{R}, -n \cdot \tfrac{f_{\max}}{R}) \quad [3]$$

Equation 3 shows that moving structures result in $R - 1$ ghost artifacts in the DC_{sub} image. The intensities of the artifacts depend on the profile of the temporal frequency spectra of the moving structures.

Origin of Temporal Filtering Effects

The aliasing artifacts that are apparent in the DC lead to errors in the coil sensitivity maps derived from DC_{sub}. In such a case the aliased signals cannot be accurately reconstructed. This causes inherent temporal filtering effects as have been observed in TSENSE image series (7). Spatial smoothing of the raw coil sensitivities reduces the level of error to some extent.

Additional temporal filtering originates from the DC subtraction procedure as often used in k-t SENSE or k-t GRAPPA, for example. The DC_{sub} signal is subtracted from the raw data $S(k_x,k_y,t)$ only at those sampled k-t positions that are given by the sampling function. The raw signal after DC subtraction can be formulated in k-t space as follows:

$$S_{-\text{DC}}(k_x,k_y,t) = E(k_x,k_y,t) \cdot (S(k_x,k_y,t) - DC_{\text{sub}}(k_x,k_y)) \quad [4]$$

After applying FT on Eq. 4, the signal can be formulated in ***r***-f space:

$$\rho_{-DC}(x,y,f) = \mathrm{PSF}(x,y,f) * (\rho_{full}(x,y,f) - DC_{sub}(x,y)) \\ = \rho_{sub}(x,y,f) - \mathrm{PSF}(x,y,f) * DC_{sub}(x,y) \quad [5]$$

The term $\mathrm{PSF}(x,y,f) * \mathrm{DC}_{sub}(x,y)$ may be interpreted as multiple replica of DC_{sub}. The PSF generates $R - 1$ additional replica of DC_{sub}, which are shifted with respect to each other (see Fig. 1c):

$$\mathrm{PSF}(x,y,f) * \mathrm{DC}_{sub}(x,y) = \rho_{sub}\left(x, y - n \cdot \frac{\mathrm{FOV}}{R}, -n \cdot \frac{f_{max}}{R}\right) \\ \text{with} \quad n = 0,\ 1,\ \ldots,\ R-1 \quad [6]$$

However, because $\mathrm{PSF}(x,y,f) * \mathrm{DC}_{sub}(x,y)$ is subtracted from $\rho_{sub}(x,y,f)$ (see Eq. 5), the signal cancels out at the temporal frequencies $n \cdot \frac{f_{max}}{R}$ with $n = 0, 1, \ldots, R - 1$. The missing temporal frequencies cannot be recovered by reconstruction algorithms and thus introduce artifacts in the reconstructed image series.

In summary, there exist two sources for temporal filtering effects in dynamic pMRI: errors in coil sensitivity maps that are derived from DC_{sub} and signal nulls in the temporal frequency spectra that are generated by subtracting DC_{sub} from the raw data.

Reduction of Temporal Filtering Effects using a GRAPPA Filter

In principle, the temporal filtering effects can be reduced significantly by estimating the unaliased DC_{full} signal. As TGRAPPA has been shown to exhibit only insignificant temporal filtering effects, we propose to estimate DC_{full} by applying GRAPPA weights (derived from DC_{sub}) on the DC_{sub} signal. This is equivalent to the performance of a TGRAPPA reconstruction and a subsequent temporal averaging of the reconstructed full FOV time frames, but it requires less computation time. It has been shown that GRAPPA can be formulated as a spatial convolution filter in the image domain (13). However, in contrast to a simple spatial low pass filter, the GRAPPA filter additionally removes aliasing artifacts and thereby yields a better estimation of the unaliased DC_{full} signal.

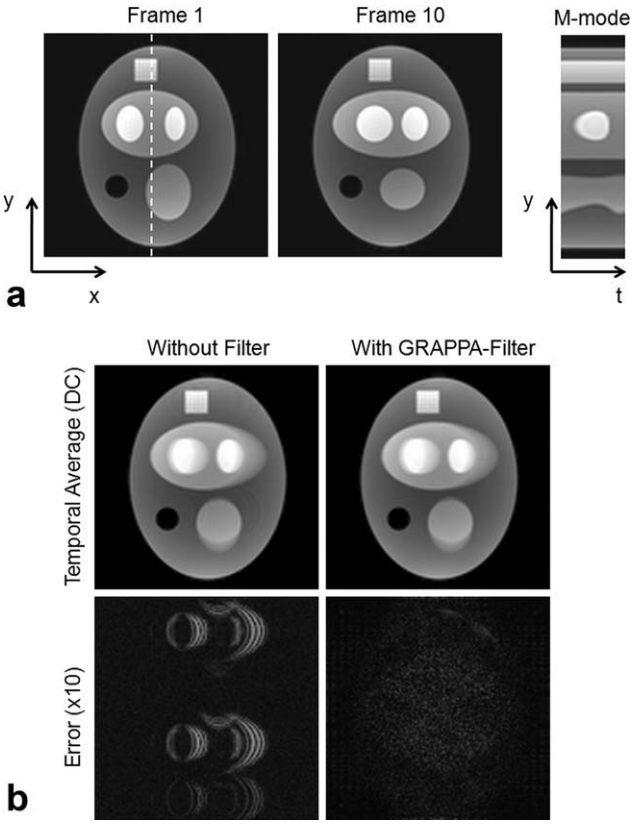

FIG. 2. **a**: Numerical dynamic phantom used in this study. Images from two time frames and the signal over time (M mode) along the dashed vertical line as indicated in the image are shown. Please note, that the dashed line in Frame 1 is not part of the phantom. **b**: In the simulation, an acceleration factor of $R = 4$ was applied along the y dimension. As predicted in the Theory section, three ($R - 1$) ghost artifacts are apparent in the unfiltered temporal average image (left column). In contrast, no errors can be seen in the GRAPPA-filtered temporal average image, but an SNR penalty due to the spatially dependent GRAPPA g-factor can be observed (right column). The error images (bottom row) are scaled by a factor of 10 for better visibility.

METHODS

Simulations

Computer simulations were performed to study the temporal filtering effects. Images from a numerical dynamic phantom (matrix size 128 × 128, 20 time frames) were multiplied with coil sensitivity maps from a circular eight-channel receive array that were obtained from Biot-Savart calculations. The images were Fourier-transformed to yield data in the *k-t* space and Gaussian white noise was added. The data were retrospectively subsampled along the k_y direction by an acceleration factor of $R = 4$. Images from the numerical phantom can be seen in Figure 2a.

To investigate temporal filtering effects due to coil sensitivity errors, TSENSE reconstructions were performed. High-resolution coil sensitivity maps (i.e., without spatial smoothing) were obtained from both unfiltered and GRAPPA-filtered DC. Regularization was not applied during image reconstruction. Temporal frequency spectra from the reconstructed image series were obtained by performing a Fourier transform along the temporal dimension and by averaging the magnitude spectra within a small region-of-interest (ROI).

The GRAPPA filter may lead to noise enhancement in the DC image due to an increased geometry factor. To study the effects of noise enhancement for coil calibration, TSENSE reconstructions were performed using different noise levels ($\sigma = 0.1$, 0.3, 1, and 3). The reconstructed images were compared to the fully sampled images. The root mean squared error of the reconstructed images was computed for an ROI (15 × 15 pixels). The mean SNR for the DC image was estimated for the same ROI according to Ref. 12 considering the noise enhancement due to the GRAPPA geometry factor (13) for the filtered DC.

In addition, *k-t* SENSE reconstructions were performed to study temporal filtering effects due to DC subtraction. Prior information about spatio-temporal correlations was obtained from 11 fully sampled training lines per time

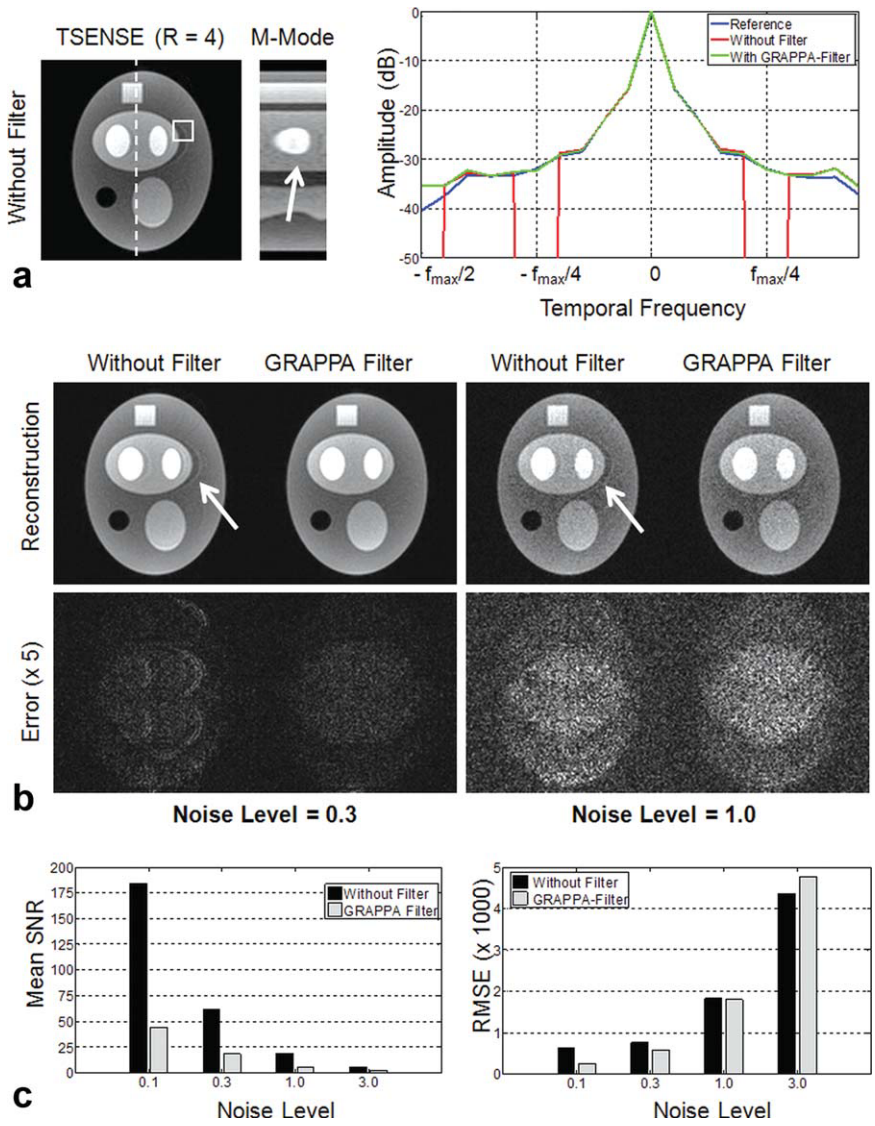

FIG. 3. Computer simulation results illustrating temporal filtering effects due to errors in the coil sensitivity maps. **a**: TSENSE reconstructions (acceleration factor $R = 4$) and the signal-over-time (M mode) along a vertical column as indicated by the dashed line in the TSENSE image are shown. The coil maps were obtained from the unfiltered DC and show undesired artifacts (see arrow). The temporal filtering effects are also reflected in form of signal nulls in the temporal frequency spectra. The spectra were obtained from a ROI as indicated by the small box in the TSENSE image. The top row in **(b)** shows TSENSE reconstructions for different noise levels and in the bottom the reconstruction errors are presented. The error images are scaled by a factor of 5 for better visibility. The reconstructions without filter exhibit artifacts (see arrows). **c**: The mean signal-to-noise ratio (SNR) in the temporal average image and the root mean squared error (RMSE) of the TSENSE reconstructions were calculated from a small ROI (15 × 15 pixels) for different noise levels. The location of the ROI is indicated by a small box in (a).

frame. The coil sensitivity maps were derived from the fully sampled data, so that temporal filtering effects due to errors in the coil sensitivity maps could be avoided. Both unfiltered and GRAPPA-filtered DC were subtracted from the raw data during data reconstruction.

Experiments

In vivo experiments were carried out on two healthy volunteers using clinical 1.5 T MRI scanners (Siemens, Erlangen, Germany) equipped with an eight-channel cardiac array (Nova Medical, Inc., Wilmington, MA) and a 32-channel cardiac array (In Vivo Corporation, Orlando, FL). Dynamic cardiac imaging was performed by using balanced steady state free precession sequences [(a.k.a. bSSFP, TrueFISP, fast imaging employing steady state acquisition (FIESTA), or fast field echo (FFE)]. The experiments were approved by the Institutional Review Board and according to the Institutional Review Board regulations, informed consent was obtained from each volunteer prior to the scan session.

The image reconstruction was done offline using Matlab (Mathworks, Natick, MA). Prior to any further processing, a noise prewhitening procedure (14) was performed to generate uncorrelated virtual channels that have noise with unit variance.

A fully sampled ECG-gated experiment was performed during breath-hold using the 32-channel array. The sequence parameters were: echo time = 1.37 msec, pulse repitition time = 2.74 msec, flip angle = 50°, FOV = 270 × 360 mm^2, slice thickness = 6 mm, matrix size = 150 × 192, 32 cardiac phases. The data set was retrospectively subsampled to simulate an accelerated acquisition ($R = 4$). Image reconstruction was performed with *k-t* SENSE using 11 training lines. To exclude errors in the coil sensitivity maps, the fully sampled data set was used for coil sensitivity calibration. The unfiltered DC as well as the GRAPPA-filtered DC were subtracted from the raw data during the image reconstruction.

An accelerated ($R = 4$) free-breathing experiment was performed using the eight-channel array. The sequence parameters were: echo time = 1.37 msec, pulse repitition time = 2.74 msec, flip angle = 50°, FOV = 270 × 360

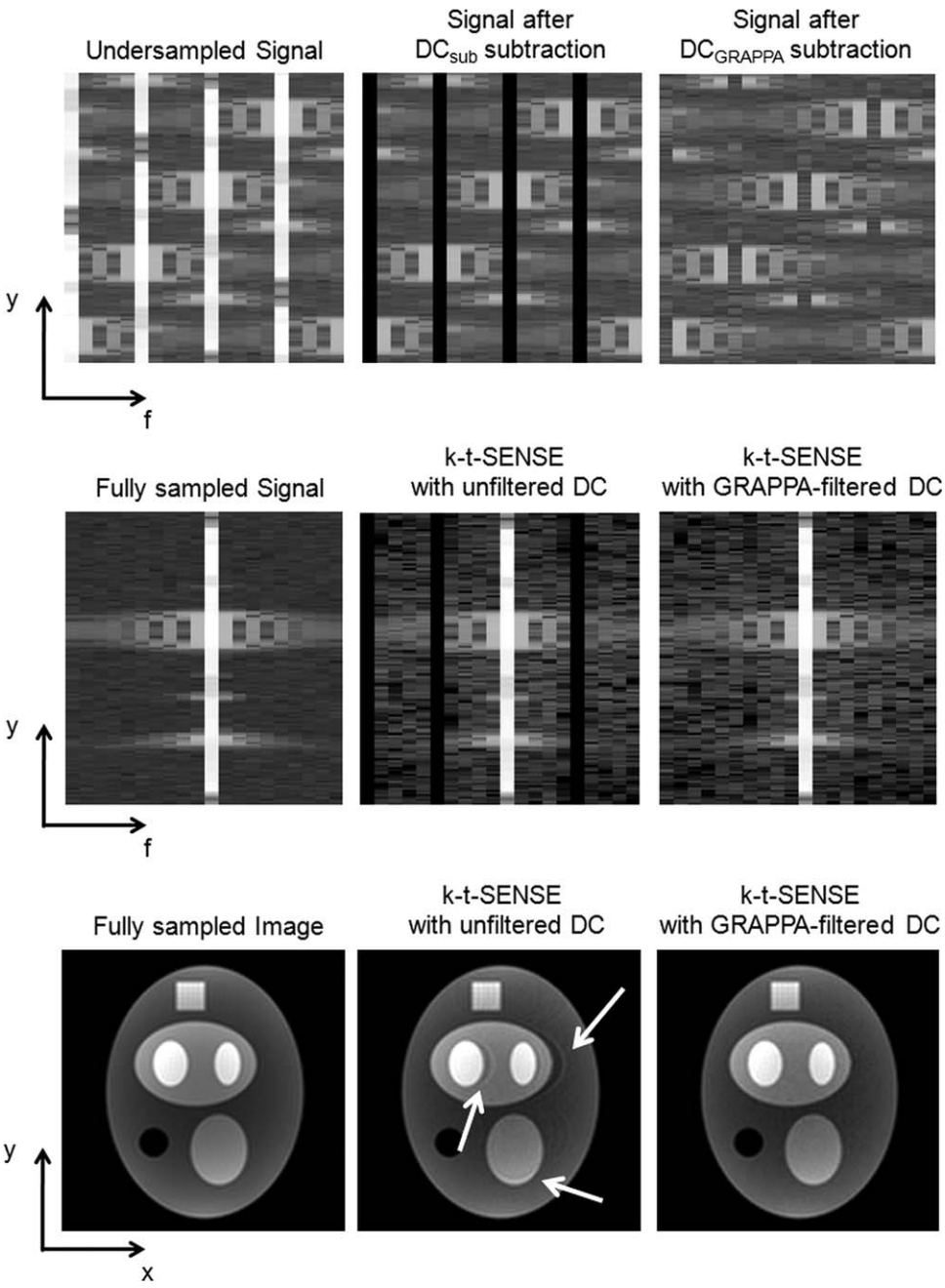

FIG. 4. Computer simulation results demonstrating the introduction of signal nulls along the temporal frequency dimension *f*. The top row shows the undersampled ($R = 4$) data in the *y-f* plane (left). When the unfiltered temporal average signal (DC_{sub}) is subtracted from the data, signal nulls can be observed at $R = 4$ positions along the temporal frequency dimension (middle). The signal nulls can be avoided when the GRAPPA-filtered temporal average signal (DC_{GRAPPA}) is subtracted from the data (right). The middle row shows the data in the *y-f* plane after *k-t* SENSE reconstruction. Except for $f = 0$, the signal nulls cannot be recovered by the reconstruction (middle). The reconstruction using the GRAPPA filter does not show the signal nulls (right). The bottom row displays an exemplary time frame reconstructed with *k-t* SENSE without (middle) and with GRAPPA filter (right). Please note that the artifacts in the *k-t* SENSE reconstruction (see arrows) are purely due to the DC_{sub} subtraction because the coil sensitivity maps are derived from the full sampled signal and thus can be assumed to be without aliasing artifacts in this example.

mm^2, slice thickness = 6 mm, matrix size = 92 × 192, 128 time frames. The images were reconstructed with TSENSE by using coil sensitivity maps that were obtained both from the unfiltered DC and from the GRAPPA-filtered DC.

RESULTS

Simulations

Errors in the DC image obtained from the subsampled data are illustrated in Figure 2b. The figure shows the unfiltered and the GRAPPA-filtered DC images from the computer simulation. In addition, the differences between unfiltered DC and DC_{full} and between GRAPPA-filtered DC and DC_{full} are presented. The DC_{full} image thereby represents the temporal average from the fully sampled data set. While errors due to aliased signal components are apparent in the unfiltered DC, no errors can be observed in the GRAPPA-filtered DC. However, spatially dependent noise enhancement can be noticed in the GRAPPA-filtered image which is typical for parallel imaging reconstructions (1,13).

The effect of errors in the coil sensitivity maps can be seen in the TSENSE-reconstructed image series (Fig. 3a). When the unfiltered DC is used for coil calibration, signal nulls become apparent in the temporal frequency spectra. The signal nulls appear at quarter band and band edge, but they disappear when the GRAPPA filter is applied. As one can see in the TSENSE images, the missing temporal frequencies lead to artifacts in the reconstructed images.

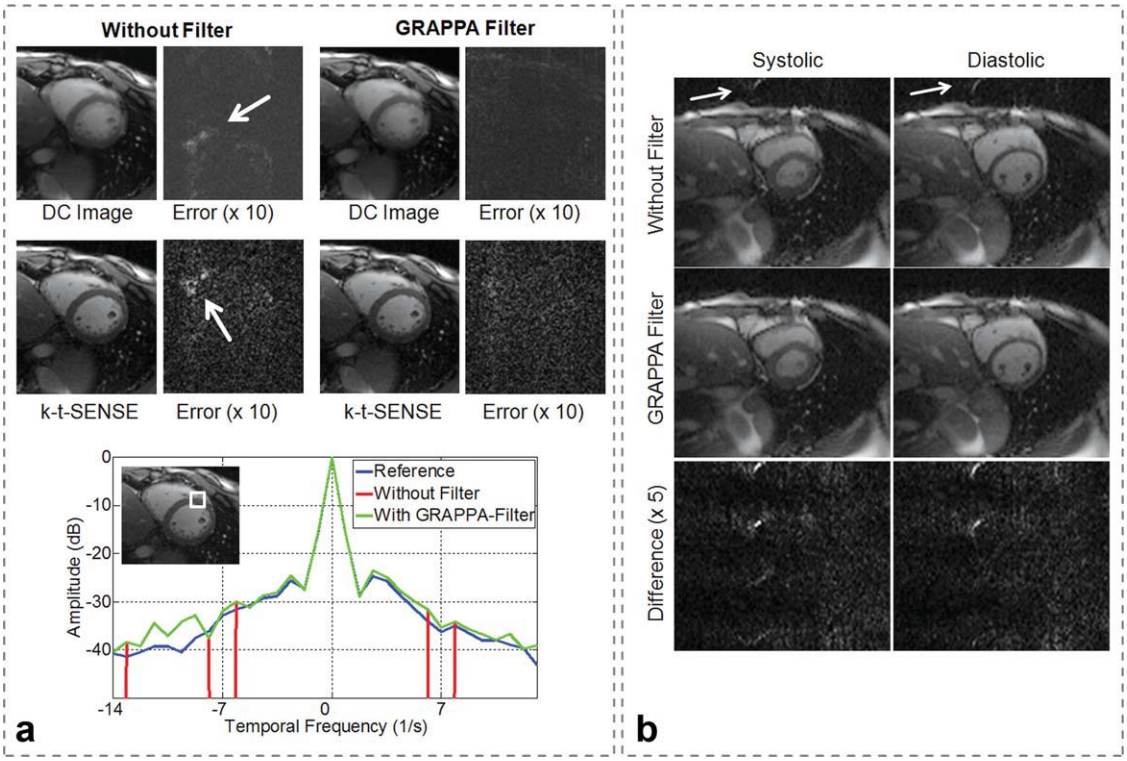

FIG. 5. Cardiac imaging results. **a**: Unfiltered and GRAPPA-filtered temporal average (DC) images are shown for a 32-channel array (acceleration factor $R = 4$). Error images illustrate differences between reconstructed DC and DC obtained from the fully sampled images. The error images are scaled by a factor of 10 for better visibility. The arrow indicates aliasing artifacts in the unfiltered DC image. In addition, *k-t* SENSE reconstructions are shown. During reconstruction, the unfiltered DC as well as the GRAPPA-filtered DC signal was subtracted from the raw data. The error images indicate differences between reconstructed and fully sampled images and are scaled by a factor of 10. Signal nulls can be observed in the temporal frequency spectra from the reconstruction with unfiltered DC. The spectra were obtained from a small region-of-interest (see box in image inset). **b:** Results from an accelerated ($R = 4$) acquisition during free breathing obtained with an eight-channel array. TSENSE reconstructions from systolic and diastolic cardiac phases are shown. The images without filter (top row) exhibit ghost artifacts as indicated by the arrows. The difference images between the reconstructions with and without GRAPPA filter are scaled by a factor of five for better visibility (bottom row). [Color figure can be viewed in the online issue, which is available at wileyonlinelibrary.com.]

The effect of noise on TSENSE image quality is shown in Figure 3b. The images for moderate and high noise levels exhibit artifacts when the unfiltered DC is used for coil sensitivity calculation. In contrast, the TSENSE images using the GRAPPA-filtered DC do not exhibit such artifacts. In addition, the noise enhancement due to the GRAPPA filter does not reduce the image quality significantly. Please note that the SNR in some regions of the GRAPPA-filtered DC image was very low (SNR $\sim$ 6 for noise level $\sigma = 1.0$; see Fig. 3c) compared to the SNR in the unfiltered DC image (SNR $\sim$ 18 for noise level $\sigma = 1.0$). Only for very high noise levels ($\sigma \sim 3.0$) the error in the TSENSE images with GRAPPA filter is increased compared to the images without filter (see Fig. 3c).

Figure 4 illustrates the introduction of signal nulls along the temporal frequency dimension when the unfiltered DC is subtracted from the undersampled data. Except for the frequency $f = 0$, the signal nulls cannot be recovered by a pMRI reconstruction such as *k-t* SENSE. The signal nulls can be avoided when the GRAPPA-filtered DC is subtracted and thus the *k-t* SENSE reconstruction will yield a better reconstruction.

Experiments

Figure 5a illustrates that the artifacts in the unfiltered DC are removed when the GRAPPA filter is applied. In this example, the noise enhancement in the GRAPPA-filtered DC is not noticeable. The artifacts in the *k-t* SENSE reconstructions without GRAPPA filter can be attributed to the signal nulls in the temporal frequency spectra.

Results from an accelerated in vivo experiment are presented in Fig. 5b. While ghost artifacts can be observed in the TSENSE images with unfiltered DC, these artifacts are not apparent in the TSENSE images with GRAPPA filter.

DISCUSSION

In TSENSE, undesired temporal filtering occurs implicitly due to small localized errors in the coil sensitivity maps that are derived from the DC image and in *k-t* SENSE additional temporal filtering is introduced by subtracting the DC from the raw data. In contrast, TGRAPPA uses inherently spatial smoothed coil sensitivity estimates and practically does not exhibit temporal

filtering effects. The reason for this is that localized errors in the DC image do not result in localized errors in the image reconstruction but might lead to a small degree of additional noise enhancement.

GRAPPA has been demonstrated to improve coil sensitivity estimation for autocalibrated SENSE-based reconstruction algorithms by enhancing the resolution of the autocalibration data (15). Here, GRAPPA is used to remove errors in the DC signal and by this means to provide better estimates of spatial coil sensitivity maps and to avoid signal nulls in the temporal frequency spectra when using DC subtraction. We have demonstrated by computer simulations and by cardiac imaging experiments that by using the GRAPPA-filtered DC, temporal filtering effects can be reduced significantly. This is particularly important when the dynamics of the objects has a broad temporal frequency spectrum. In particular, fast moving tissue with high signal intensity (such as fat in cardiac imaging experiments using SSFP sequences) can cause significant errors in the DC image.

As has been demonstrated by computer simulations with varying noise level, the noise enhancement due to the GRAPPA filter does not significantly reduce the image quality. This can be explained because the SNR of the DC image is generally higher than the SNR of a single time frame. Thus, there should be sufficient SNR for accurate coil sensitivity calibration because otherwise the SNR of the reconstructed time frames might not be sufficient for providing images with diagnostic value. However, in the case of very high acceleration factors (and hence very low SNR values) further improvements might include polynomial or other fitting procedures (as presented in Ref. 1) on the GRAPPA-filtered DC image to mitigate the negative effects of noise for coil sensitivity calibration. Thus, it can be said that the SNR in the filtered DC image (and not the geometry factor alone) is the limiting factor for the performance of the GRAPPA filter.

In *k-t* SENSE, a VD sampling scheme is often applied to acquire the training data interleaved with the undersampled data. In principle, both training and undersampled data can be used to compute the DC image. In that way, the errors in the DC image could be corrected to some extent. However, this approach does not guarantee a sufficient suppression of errors in the DC image because moving structures are typically represented by higher spatial frequencies.

Although it is not clear if DC subtraction is generally used in *k-t* SENSE, it is used in other dynamic pMRI approaches. For example, DC subtraction has been shown to improve the image quality in *k-t* GRAPPA reconstructions (6). In addition, DC subtraction is useful when the FOV is not appropriately chosen so that prefolding artifacts occur in the full FOV (16,17). For example, in dynamic cardiac MRI the chest wall which normally contains the prefolding artifacts can be considered to be static and therefore it is removed prior to the reconstruction.

CONCLUSIONS

When deriving the DC signal by averaging the time frames from a dynamic image series, aliasing artifacts are introduced in the DC image. These artifacts lead to undesired temporal filtering effects when the DC image is used for coil sensitivity calibration or when the DC signal is subtracted from the raw data. By applying a GRAPPA filter to the DC signal, the temporal filtering effects can be reduced significantly and in this way result in a better image quality and a better temporal fidelity in TSENSE and *k-t* SENSE reconstructions.

ACKNOWLEDGMENT

The authors thank Shaihan Malik for providing the numerical phantom.

REFERENCES

1. Pruessmann KP, Weiger M, Scheidegger MB, Boesiger P. SENSE: sensitivity encoding for fast MRI. Magn Reson Med 1999;42:952–962.
2. Griswold MA, Jakob PM, Heidemann RM, Nittka M, Jellus V, Wang J, Kiefer B, Haase A. Generalized autocalibrating partially parallel acquisitions (GRAPPA). Magn Reson Med 2002;47:1202–1210.
3. Kellman P, Epstein FH, McVeigh ER. Adaptive sensitivity encoding incorporating temporal filtering (TSENSE). Magn Reson Med 2001; 45:846–852.
4. Breuer FA, Kellman P, Griswold MA, Jakob PM. Dynamic autocalibrated parallel imaging using temporal GRAPPA (TGRAPPA). Magn Reson Med 2005;53:981–985.
5. Tsao J, Boesiger P, Pruessmann KP. k-t BLAST and k-t SENSE: dynamic MRI with high frame rate exploiting spatiotemporal correlations. Magn Reson Med 2003;50:1031–1042.
6. Huang F, Akao J, Vijayakumar S, Duensing GR, Limkeman M. k-t GRAPPA: a k-space implementation for dynamic MRI with high reduction factor. Magn Reson Med 2005;54:1172–1184.
7. Madore B. UNFOLD-SENSE: a parallel MRI method with self-calibration and artifact suppression. Magn Reson Med 2004;52:310–320.
8. Malik SJ, Schmitz S, O'Regan D, Larkman DJ, Hajnal JV. x-f choice: reconstruction of undersampled dynamic MRI by data-driven alias rejection applied to contrast-enhanced angiography. Magn Reson Med 2006;56:811–823; Erratum in: Magn Reson Med 2007;57:813.
9. Hansen MS, Atkinson D, Sorensen TS. Cartesian SENSE and k-t SENSE reconstruction using commodity graphics hardware. Magn Reson Med 2008;59:463–468.
10. Xu D, King KF, Liang ZP. Improving k-t SENSE by adaptive regularization. Magn Reson Med 2007;57:918–930.
11. Chao TC, Chung HW, Hoge WS, Madore B. A 2D MTF approach to evaluate and guide dynamic imaging developments. Magn Reson Med 2010;63:407–418.
12. Kellman P, McVeigh ER. Image reconstruction in SNR units: a general method for SNR measurement. Magn Reson Med 2005;54:1439–1447; Erratum in: Magn Reson Med 2007;58:211–212.
13. Breuer FA, Kannengiesser SA, Blaimer M, Seiberlich N, Jakob PM, Griswold MA. General formulation for quantitative G-factor calculation in GRAPPA reconstructions. Magn Reson Med 2009;62:739–746.
14. Pruessmann KP, Weiger M, Börnert P, Boesiger P. Advances in sensitivity encoding with arbitrary k-space trajectories. Magn Reson Med 2001;46:638–651.
15. Hoge WS, Brooks DH. Using GRAPPA to improve autocalibrated coil sensitivity estimation for the SENSE family of parallel imaging reconstruction algorithms. Magn Reson Med 2008;60:462–467.
16. Goldfarb JW. The SENSE ghost: field-of-view restrictions for SENSE imaging. J Magn Reson Imaging 2004;20:1046–1051.
17. Griswold MA, Kannengiesser S, Heidemann RM, Wang J, Jakob PM. Field-of-view limitations in parallel imaging. Magn Reson Med 2004; 52:1118–1126.